TRENDS IN SCIENCES 2026; 23(2): 11604
https://doi.org/10.48048/tis.2026.11604 RESEARCH ARTICLE

Hydrothermal-Assisted Synthesis of Mullite Ceramics from Industrial Byproducts: Phase and Microstructure Evolution

Destia Nurika[1,3], Limson Elismen Sihombing[5], Felli Rusumayanti[2,4], Febiyanto[2], Shokhul Lutfi[2], Jayadi[2], Agus Sukarto Wismogroho[1], Wahyu Bambang Widayatno[2], Muhamad Ikhlasul Amal[1] and Budhy Kurniawan[3,*]

[1]*Research Center for Nanotechnology Systems National Research and Innovation Agency (BRIN), South Tangerang 15314, Indonesia*
[2]*Research Center for Advanced Material National Research and Innovation Agency (BRIN), South Tangerang 15314, Indonesia*
[3]*Department of Physics, Universitas Indonesia, Depok 16424, Indonesia*
[4]*Department of Chemical Engineering, Universitas Indonesia, Depok 16424, Indonesia*
[5]*Department of Physics, Universitas Sumatera Utara, Medan 20155, Indonesia*

([*]Corresponding author's e-mail: budhy.kurniawan@sci.ui.ac.id)

Received: 16 August 2025, Revised: 1 September 2025, Accepted: 10 September 2025, Published: 10 November 2025

Abstract

This study presents a sustainable route for synthesizing high-performance mullite ceramics using aluminum dross and kaolin, with a focus on enhancing precursor reactivity through hydrothermal pretreatment. Three compositions were evaluated: MC (commercial alumina + kaolin), MD (untreated dross + kaolin) and MH (hydrothermally treated dross + kaolin). Hydrothermal treatment at 200 °C for 24 h effectively removed soluble impurities (e.g., NaCl, AlN) and converted non-oxide phases into reactive Al_2O_3 (e.g., $2AlN+3H_2O \rightarrow Al_2O_3+2NH_3$), increasing the alumina content from 70.252 to 71.803 wt%. X-ray diffraction revealed enhanced mullite crystallinity in MD and MH, attributed to fluxing oxides such as Fe_2O_3 and MgO that promoted liquid-phase sintering and reduced activation energy. Scanning electron microscopy confirmed that MH exhibited a denser microstructure with well-developed mullite whiskers (~12.25 µm). At 1,500 °C, MH achieved superior mechanical properties with compressive strength of 110.48 MPa, porosity of 2.90% and bulk density of 2.30 g/cm³, surpassing both MD (79.01 MPa, 3.10%, 1.92 g/cm³) and MC (23.42 MPa, 11.38%, 1.61 g/cm³). These results demonstrate that hydrothermal pretreatment significantly improves phase compatibility and densification. Beyond material performance, this approach offers a scalable pathway for valorizing industrial waste, advancing circular economy practices and supporting environmentally friendly ceramic manufacturing.

Keywords: Aluminum dross, Kaolin, Alumina, Hydrothermal pretreatment, Ceramics, Impurities, Mullite

Introduction

Mullite ($3Al_2O_3 \cdot 2SiO_2$) is a high-performance aluminosilicate based ceramic renowned for its high melting point (> 1,850 °C), low thermal expansion coefficient (~2×10^{-6} K^{-1} to 5×10^{-6} K^{-1}), excellent mechanical strength under thermal stress (flexural strength ~200 - 300 MPa), and thermal shock resistance up to approximately 800 °C [1-7]. Despite its natural occurrence, mullite is rarely found in sufficient quantities or purity for industrial use, necessitating synthetic production through controlled solid-state reactions between alumina and silica sources [8]. The conventional synthesis route typically employs high-purity commercial alumina and silica, which significantly increases production costs. In response, recent research has focused on identifying alternative, sustainable raw materials that can yield mullite with

comparable performance characteristics while reducing both environmental impact and manufacturing expenses [9-12]. Several studies utilizing industrial byproducts such as mine tailings [13], coal gangue [14] and marble waste [15] for mullite synthesis have successfully confirmed the formation of prismatic α-mullite crystals and their increased presence with elevated sintering temperatures [13].

Among potential substitutes, aluminum dross a byproduct of aluminum smelting has garnered attention due to its high aluminum content, primarily in the form of Al_2O_3, AlN and unreacted metallic Al, alongside minor phases such as nitrides and oxides of magnesium and calcium [16-20]. Kaolin, a naturally abundant clay mineral rich in SiO_2 and Al_2O_3, complements aluminum dross as a secondary source of aluminosilicate components for mullite synthesis [21,22]. The utilization of these two waste-derived feedstocks offers a viable pathway for resource recovery while enabling the production of high-value ceramics. Nevertheless, the heterogeneous composition of aluminum dross can hinder mullitization by introducing foreign oxide phases that may either suppress mullite formation or degrade final product quality [23]. Intriguingly, certain impurities such as MgO, Fe_2O_3 and CaO have been reported to act as fluxing agents during sintering, promoting liquid-phase formation that facilitates densification and enhances grain growth kinetics [10,24]. Studies on various kaolin mixtures for mullite production indicate that both calcination temperature and the presence of impurities (such as Fe_2O_3 and K_2O) significantly influence mullite formation kinetics and microstructure evolution, with certain impurity profiles promoting liquid-phase sintering and enhanced densification [25].

Various pre-treatment methods have been explored to mitigate the adverse effects of impurities in aluminum dross, including acid leaching, alkaline digestion and thermal treatments. While effective in removing contaminants, these approaches often result in substantial loss of aluminum values up to 56.2% in some cases and generate secondary waste streams that require further treatment [23,26]. For example, the addition of MgO to secondary aluminum dross (SAD) was shown to improve refractory properties but introduced economic constraints due to increased raw material costs [27]. The in-situ formation of mullite is a complex solid-state reaction process significantly influenced by the characteristics and purity of Al_2O_3 and SiO_2 sources, with even small amounts of low-melting-point impurities impacting densification, grain growth and the overall microstructure and mechanical properties of alumina-mullite ceramics [28]. These challenges underscore the need for an environmentally benign and economically viable processing strategy that preserves the reactivity of aluminum-bearing phases while minimizing deleterious elements.

Hydrothermal treatment an aqueous process conducted under elevated temperature and pressure emerges as a promising solution. This method effectively removes soluble impurities such as NaCl and converts non-oxide species like AlN into reactive Al_2O_3 via hydrolysis reactions (e.g., $2AlN + 3H_2O \rightarrow Al_2O_3 + 2NH_3$), without generating acidic or basic effluents [27]. Investigations into low-temperature synthesis of mullite-based ceramics have demonstrated that industrial byproducts like marble waste can act as effective sintering aids, promoting the complete transformation of precursor minerals into mullite and significantly enhancing mechanical strength [15]. Furthermore, the strategic incorporation of mullite as an enhancer in multiphase ceramic composites, alongside heat stabilizers such as MgO, has been shown to improve mechanical properties through crack deflection and enhance densification, leading to high flexural strength and low porosity [29]. By enhancing the alumina content and reactivity of dross, hydrothermal pretreatment potentially improves its compatibility with kaolin for mullite synthesis. To date, no systematic study has compared mullite synthesized from hydrothermally treated aluminum dross and kaolin against untreated counterparts and commercial alumina-based controls.

This study aims to fill this gap by investigating the influence of hydrothermal pretreatment on the phase evolution, microstructural development, and mechanical behavior of mullite produced via solid-state sintering. Particular emphasis is placed on evaluating the effectiveness of hydrothermal processing in reducing impurity content and optimizing mullitization kinetics across a range of sintering temperatures (950 - 1,500 °C). The findings contribute to the development of a scalable, eco-friendly methodology for synthesizing high-performance mullite ceramics from industrial

waste materials, aligning with the principles of the circular economy and sustainable manufacturing goals.

Materials and methods

Raw materials and sample preparation

Aluminum dross, an industrial byproduct from aluminum smelting (Jombang, Indonesia), kaolin from Bangka Belitung and commercial alumina (99.4% purity, West Kalimantan, Indonesia) were utilized as the primary starting materials for mullite synthesis. To ensure reactivity and homogeneity, all raw materials were mechanically sieved to achieve a particle size of ≤ 325 mesh (≤ 45 μm). Three distinct stoichiometric compositions, designed to yield mullite ($3Al_2O_3{\cdot}2SiO_2$), were prepared for comparative analysis:

1) MC: Composed of commercial alumina and kaolin.

2) MD: Prepared using as-received aluminum dross and kaolin.

3) MH: Incorporating hydrothermally pretreated aluminum dross and kaolin.

For the MH composition, a hydrothermal pretreatment was applied to the aluminum dross to enhance its reactivity and reduce impurity content. This process involved mixing the dross with deionized water at a solid-to-liquid ratio of 1:3 (w/w). The mixture was then subjected to hydrothermal conditions at 200 °C for 24 h in a sealed autoclave. This specific treatment facilitated the hydrolysis of non-oxide phases, such as aluminum nitride (AlN), into highly reactive aluminum oxide ($2AlN + 3H_2O \rightarrow Al_2O_3 + 2NH_3$), while simultaneously dissolving soluble impurities like sodium chloride (NaCl). Following hydrothermal treatment, the treated residue was thoroughly dried at 120 °C for 3 h before being integrated into the sample preparation.

Each formulated composition was then subjected to thorough homogenization via ball-milling in a planetary mill. A milling speed of 300 rpm was maintained for 3 h, utilizing 50 mL of deionized water as the milling medium to ensure intimate mixing of the precursor powders. The resulting homogeneous slurries were subsequently dried at 110 °C for 1 h to eliminate residual moisture, yielding fine, dry powders. To prepare green bodies for sintering, these powders were uniaxially pressed into cylindrical pellets, each measuring 18.3 mm in diameter and 20 mm in thickness, under a controlled pressure of 10 MPa to ensure consistent green density across all samples.

Sintering

The prepared green pellets were subjected to a precisely controlled sintering regimen across a range of temperatures: 950, 1,100, 1,300 and 1,500 °C. A consistent dwell time of 2 h was maintained at each peak temperature, with a uniform heating and cooling rate of 10 °C/min. All sintering procedures were conducted in a controlled atmosphere furnace. These specific temperature intervals were thoughtfully determined to enable comprehensive monitoring of phase evolution, densification behavior, and microstructural development throughout the critical stages of mullitization. Post-sintering, samples were allowed to cool naturally within the furnace, a slow cooling process designed to mitigate thermal shock-induced microcracking and preserve the structural integrity of the ceramic body.

Characterization

The chemical composition of both the raw materials and the final sintered products was quantitatively determined using X-ray fluorescence spectroscopy (XRF, Bruker S2 PUMA). Phase identification and assessment of crystalline purity were performed using X-ray diffraction (XRD, SMARTLAB RIGAKU) with Cu-Kα radiation generated at 30 mA and 40 kV. Relative crystallinity was quantitatively evaluated by calculating the ratio of integrated peak intensities corresponding to the identified crystalline phases against the total scattering intensity.

Physical properties, including bulk density and apparent porosity, were precisely measured utilizing the Archimedes method, with deionized water serving as the immersion medium, following ASTM B962 – 15 standards. The compressive strength of the sintered cylindrical pellets was determined using a universal testing machine (ASTM C565), applying a consistent crosshead speed of 1.0 mm/min. Five samples were tested to obtain the average and standard deviation. Microstructural characteristics, including grain morphology and elemental distribution, were meticulously analyzed using scanning electron microscopy coupled with energy-dispersive X-ray spectroscopy (SEM-EDX, Jeol JSM-IT200).

Results and discussion

Characterization of starting materials

The systematic evaluation of mullite synthesis from alternative raw materials involved a comprehensive analysis of chemical composition, phase evolution, microstructural development and mechanical performance. The findings robustly demonstrate the efficacy of hydrothermal pretreatment in augmenting aluminum dross reactivity, thereby promoting the formation of high-quality mullite under conventional solid-state sintering conditions.

Table 1 Chemical composition of kaolin, alumina and aluminum dross.

Compound	Content (wt%)			
	Kaolin	Aluminum dross	Aluminum dross hydrothermal	Commercial alumina
Al_2O_3	46.90	70.25	71.80	99.40
SiO_2	48.60	9.42	9.90	-
Fe_2O_3	1.20	4.39	3.83	-
MgO	1.10	4.12	4.28	-
Na_2O	0.20	2.35	2.50	-
K_2O	0.50	1.30	1.05	-
CaO	0.10	0.83	0.81	-
P_2O_5	0.46	0.43	0.32	0.38
ZnO	-	0.29	0.27	-
TiO_2	-	0.42	0.39	-
Other	0.94	6.2	4.85	0.22

X-ray fluorescence (XRF) analysis shown in **Table 1** provided critical insights into the initial compositional differences among the raw materials. Kaolin exhibited a near-stoichiometric SiO_2–Al_2O_3 ratio (48.60 wt% SiO_2 and 46.90 wt% Al_2O_3), confirming its suitability as a primary silicate source for mullite synthesis. Commercial alumina, with its high purity (99.408 wt% Al_2O_3), served as an essential benchmark for comparative performance. In contrast, untreated aluminum dross presented a more complex composition, comprising 70.252 wt% Al_2O_3 alongside significant concentrations of impurities such as Fe_2O_3 (4.390 wt%) and MgO (4.116 wt%). These impurities are known to exert a profound influence on reaction kinetics and the ultimate properties of the sintered product. Following hydrothermal treatment of the aluminum dross at 200 °C for 24 h (with a 1:3 solid-to-liquid ratio), a notable compositional shift was observed: The Al_2O_3 content slightly increased to 71.803 wt%, while Fe_2O_3 decreased to 3.833 wt% and MgO remained relatively stable at 4.281 wt%. This advantageous compositional alteration is primarily ascribed to the dissolution of soluble phases, notably NaCl and the in-situ conversion of non-oxide species, such as aluminum nitride (AlN), into more reactive Al_2O_3 through aqueous hydrolysis reactions (i.e., $2AlN + 3H_2O \rightarrow Al_2O_3 + 2NH_3$) [30-33]. These crucial modifications not only improved the stoichiometric compatibility of the dross with kaolin but also significantly enhanced its overall reactivity, which was subsequently evidenced by the denser microstructure and superior mechanical strength achieved in the MH samples [34].

Phase composition of the sample

Figure 1 presents the X-ray diffraction (XRD) patterns of mullite ceramic with different alumina sources, recorded across the entire sintering temperature range (950 - 1,500 °C), offered a detailed mechanistic understanding of the mullitization progression. At 950 °C, all compositions predominantly displayed characteristic corundum peaks (square, ■), with a complete absence of detectable mullite (star, *), indicating that this temperature was insufficient to initiate the formation of aluminosilicate phases. By 1,100 °C, faint mullite reflections emerged, signifying the incipient stages of solid-state diffusion-driven phase

transformation. As the temperature increased to 1,300 °C, mullite peak intensities became significantly more pronounced, particularly in the MD (**Figure 1(b)**) and MH (**Figure 2**) samples, although residual corundum remained visible in the MC (**Figure 1(a)**) composition. Furthermore, the presence of cristobalite (circle, ●) in the MC sample at this temperature suggested incomplete reaction kinetics, likely attributable to the intrinsically lower reactivity of commercial alumina compared to the dross-derived sources. Upon reaching the peak sintering temperature of 1,500 °C, mullite became the overwhelmingly dominant phase across all compositions, albeit with discernible variations in the degree of crystallinity. Critically, both MD and MH samples exhibited markedly higher mullite peak intensities than MC, indicative of an accelerated and more complete phase formation. This enhancement is largely attributed to the synergistic presence of fluxing oxides specifically Fe_2O_3 and MgO which effectively lowered the activation energy barrier for mullitization by facilitating the formation of transient liquid phases. These liquid phases, in turn, promoted rapid mass transport and enhanced grain boundary diffusion, thereby accelerating the reaction kinetics [35,36]. Among the dross-containing compositions, MH (**Figure 2**) displayed the most pronounced improvement in mullite crystallinity, likely due to the combined effects of reduced impurities, higher effective Al_2O_3 purity and enhanced surface reactivity directly resulting from the hydrothermal pretreatment.

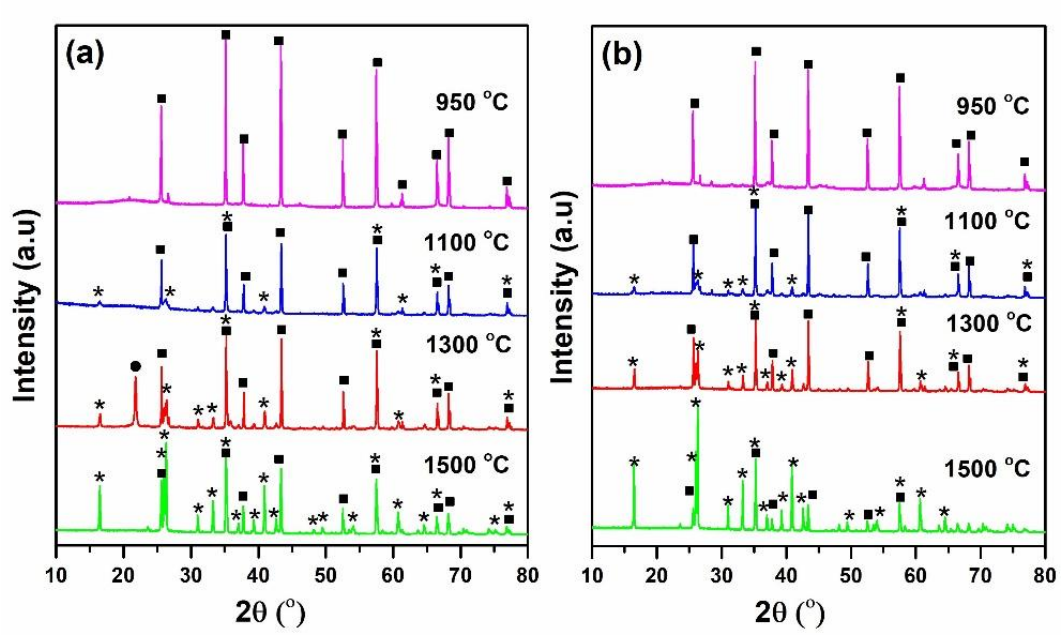

Figure 1 X-ray diffraction of mullite ceramic with different alumina sources of (a) MC and (b) MD, respectively. Signs of square (■), circle (●) and star (*) were corundum, cristobalite and mullite, respectively.

The crucial role of hydrothermal treatment in elevating dross quality was further substantiated through a comparative analysis of phase evolution and the resultant mechanical behavior. In stark contrast to conventional acid or alkaline leaching methods, which frequently lead to substantial aluminum loss (ranging from 13% to 56%) and generate hazardous waste streams [23,26]. Hydrothermal processing proved highly effective in preserving the valuable metallic content while simultaneously removing undesirable constituents. The high-pressure aqueous environment inherent to hydrothermal treatment promoted the recrystallization of alumina phases, consequently increasing their specific surface area and intrinsic reactivity. This enhanced reactivity is overtly evident in the MH samples, which, as observed through XRD, exhibited sharper mullite diffraction peaks and microscopically, more developed whisker structures compared to the MD samples. Although the hydrothermal process requires autoclave operation and

an extended treatment duration (24 h), it notably circumvents the use of aggressive chemical reagents and substantially reduces secondary pollution, thereby aligning robustly with established principles of green chemistry [27].

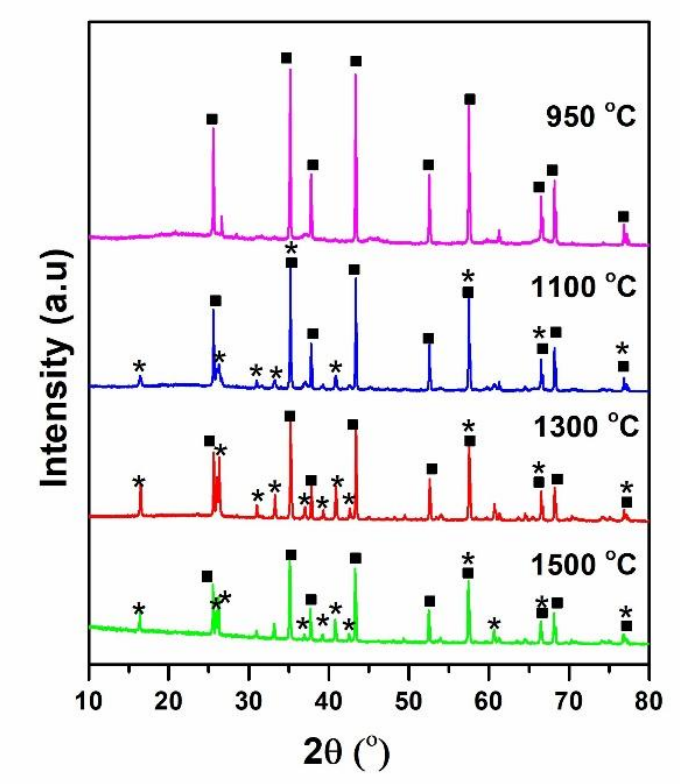

Figure 2 X-ray diffraction of MH sample. Signs of square (■) and star (*) were corundum and mullite, respectively.

The mechanism of mullite formation was discerned to vary significantly depending on the nature of the alumina source and the intrinsic presence of fluxing agents. In systems employing either commercial alumina (MC) or untreated dross (MD), kaolin underwent dehydroxylation at temperatures exceeding 600 °C, leading to the formation of amorphous SiO_2 and Al_2O_3 (Eq. (1): $Al_2Si_2O_5(OH)_4 \rightarrow Al_2O_3 + 2SiO_2 + 2H_2O$) [35]. These highly reactive intermediate phases subsequently combined with the external alumina at elevated temperatures (1,100 - 1,500 °C) to form mullite via solid-state diffusion (Eq. (2): $3Al_2O_3 + 2SiO_2 \rightarrow 3Al_2O_3{\cdot}2SiO_2$) [36]. Within the MD composition, the inherent presence of Fe_2O_3 and MgO facilitated the formation of a low-viscosity liquid phase during sintering. This transient liquid acted as an efficient medium for accelerated ion mobility and enhanced grain growth [37]. For the MH samples, hydrothermal pretreatment introduced additional, highly beneficial reaction pathways as illustrated in **Figure 3**. Non-oxide components such as AlN were effectively converted into Al_2O_3 through hydrolysis (Eq. (3): $2AlN + 3H_2O \rightarrow Al_2O_3 + 2NH_3$), while residual metallic Al reacted with water to form aluminum hydroxide, $Al(OH)_3$ (Eq. (4): $2Al + 6H_2O \rightarrow 2Al(OH)_3 + 3H_2$), which subsequently dehydrated into Al_2O_3 (Eq. (5): $2Al(OH)_3 \rightarrow Al_2O_3 + 3H_2O$). This sequence of transformation yielded a significantly more reactive alumina source characterized by a higher surface area, thereby accelerating the kinetics of Eq. (2) and leading to a more complete mullitization. Consequently, MH samples consistently exhibited greater crystallinity, reduced porosity and a markedly denser microstructure compared to the other compositions.

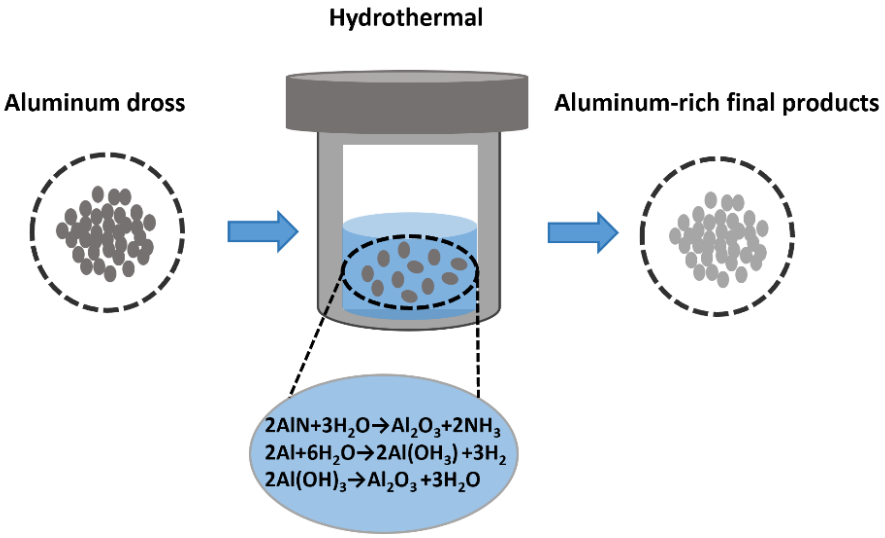

Figure 3 Mechanistic schematic of the hydrothermal transformation pathway of aluminum dross.

These findings are further supported by the crystallite size and microstrain analysis of samples sintered at 1,500 °C, as shown in **Figure 4**. Mullite synthesized from aluminum dross demonstrated greater crystallite growth compared to that derived from commercial alumina, with average crystallite sizes of 714.3 nm (MH), 709.22 nm (MD) and 689.7 nm (MC). This behavior confirms that fluxing impurities such as Fe_2O_3 and MgO in aluminum dross effectively lower the diffusion activation energy and promote crystallite growth during sintering, while hydrothermal pretreatment enhances the reactivity of alumina and accelerates mullite nucleation. In line with these results, the microstrain analysis revealed that MH exhibited the lowest lattice strain (3.9×10^{-4}), followed by MD (4.5×10^{-4}), whereas MC showed the highest value (9.3×10^{-4}). The reduction in microstrain reflects fewer lattice imperfections due to advanced crystallite growth and improved structural ordering of mullite. Taken together, the larger crystallite size and lower microstrain in MH confirm that hydrothermal pretreatment not only improves alumina reactivity but also produces mullite with higher crystallinity, reduced porosity, and superior microstructural quality.

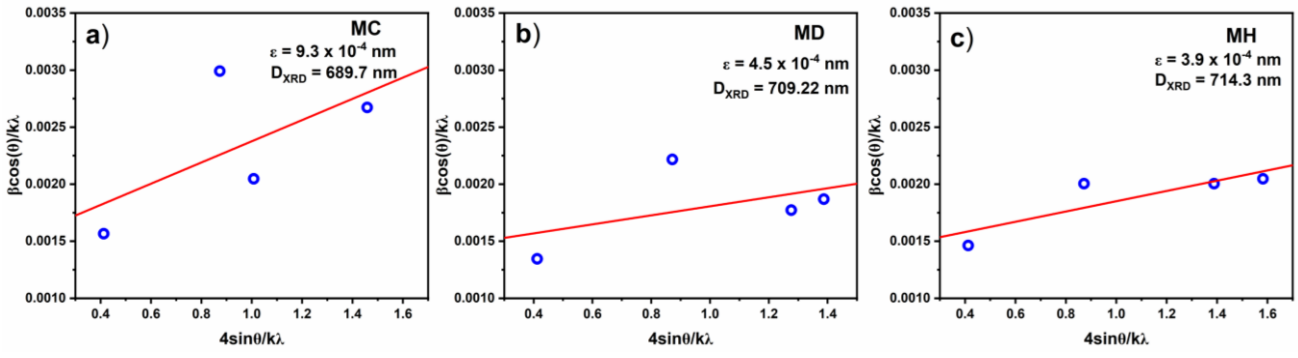

Figure 4 Crystallite size and strain from Williamson–Hall plots of mullite samples sintered at 1,500 °C: (a) MC, (b) MD, and (c) MH.

Microstructure analysis of the sample

Microstructural observations in **Figure 5**, conducted via Scanning Electron Microscopy (SEM), further corroborated the pronounced beneficial impact of hydrothermal pretreatment. SEM images of MC samples (**Figures 5(b) - 5(e)**) sintered at 1,500 °C

revealed the presence of relatively short mullite whiskers (~2.950 μm) and a notable abundance of pores, indicative of limited densification and slower grain growth kinetics. In stark contrast, both MD and MH samples displayed significantly longer whiskers (averaging 11.332 μm and 12.253 μm, respectively, as shown in **Figures 5(f)** and **5(g)** embedded within a more compact ceramic matrix, with MH exhibiting the most pronounced densification. The intrinsic presence of fluxing impurities such as Fe_2O_3 and MgO in both MD (**Figure 5(c)**) and MH (**Figure 5(d)**) compositions critically contributed to liquid-phase sintering, which effectively reduced interfacial tension and actively promoted whisker elongation and advantageous alignment [38-40]. Consistently, the particle size distribution analysis (**Figures 5(e) - 5(g)**) shows that MH exhibits a narrower and more symmetric distribution, indicating more uniform whisker growth and higher microstructural homogeneity. In contrast, MD and especially MC display broader and more heterogeneous distributions, reflecting uneven whisker development. Moreover, the superior microstructure observed in MH strongly suggests that hydrothermal treatment not only efficiently removed detrimental impurities but also beneficially modified the morphology of the alumina phases, thereby favoring rapid nucleation and subsequent growth of well-developed mullite crystals. XRD analysis additionally confirmed the persistence of unreacted corundum grains in MC and MD samples, whereas MH exhibited minimal residual alumina, providing strong evidence for more complete reaction and superior phase homogenization.

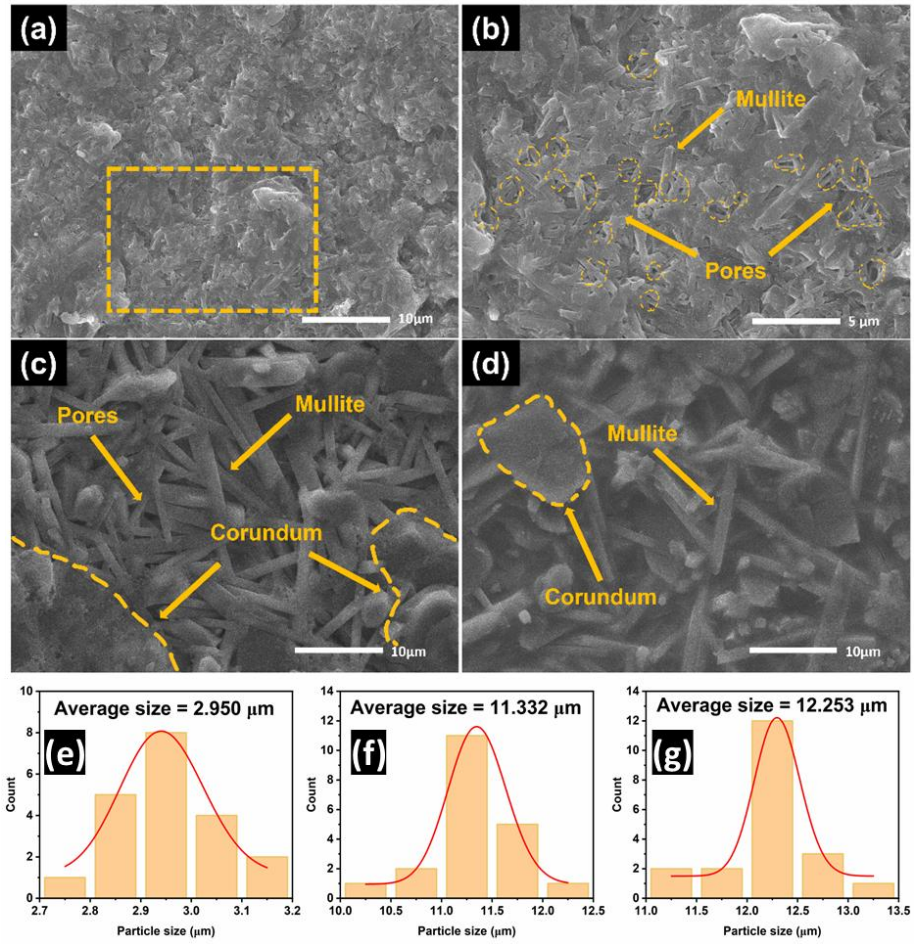

Figure 5 SEM images of sintered samples at 1,500 °C: (a) MC; (b) zoomed-in MC showing pores and short mullite whiskers; (c) MD with elongated mullite and corundum phases; (d) MH showing dense microstructure of mullite; Particle size distributions of the mullite: (e) MC; (f) MD; and (g) MH.

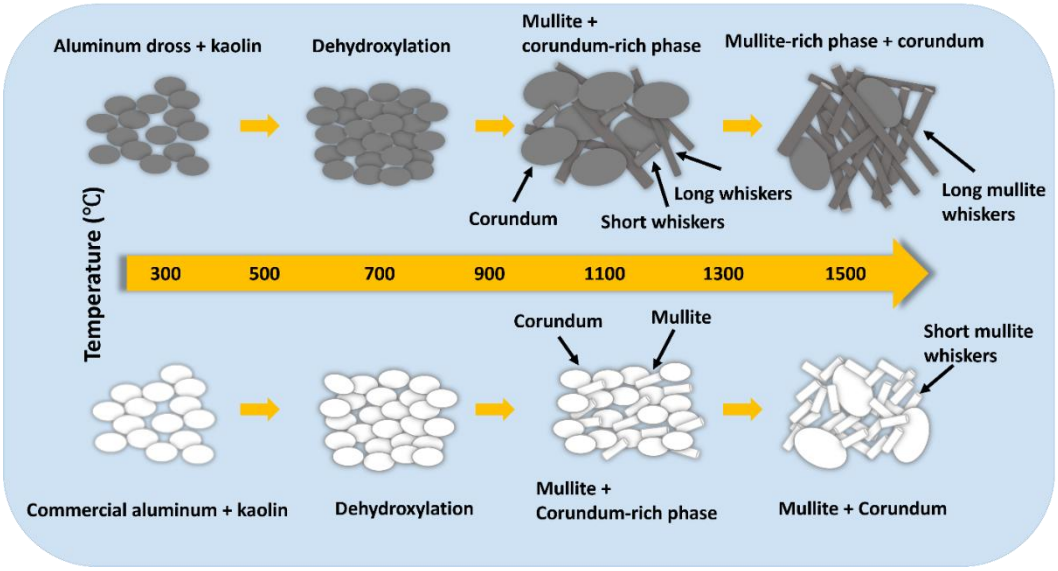

Figure 6 Schematic illustration of microstructural evolution and whisker growth in mullite from aluminum dross + kaolin and commercial alumina + kaolin.

Figure 6 illustrates the schematic microstructure evolution and whisker growth of mullite synthesized from aluminum dross-kaolin and commercial alumina-kaolin mixtures. At temperatures below approximately 600 °C, both mixtures undergo initial drying processes. Upon exceeding 600 °C, the raw materials undergo dehydroxylation, resulting in the formation of highly reactive amorphous silica and alumina. At 1,100 °C, these amorphous phases react via solid-state diffusion to form initial mullite. A distinct difference in the reaction pathway and microstructure development was observed between the two alumina sources. The sample derived from aluminum dross began forming long mullite whiskers, although the phase assemblage remained predominantly corundum. In contrast, the mixture with commercial alumina exhibited slower whisker growth, yielding only short whiskers at this stage. This divergence became more pronounced at 1,500 °C. In the dross-based sample, the mullite whiskers underwent significant further development. The presence of residual corundum phase indicates an excess of alumina that could not be incorporated into the mullite structure due to the stoichiometric limitations of the reaction. Conversely, mullite growth in the commercial alumina sample remained suboptimal, as shown in **Figure 5**. This is attributed to the absence of fluxing agents (e.g., Fe_2O_3, MgO), which are naturally present in aluminum dross and are known to enhance kinetic rates by promoting liquid-phase sintering, thereby facilitating the nucleation and growth of well-developed mullite whisker crystallites as shown in **Figure 4**.

Mechanical properties of the samples

The observed mechanical property measurements provided compelling quantitative support for the microstructural and phase findings. As detailed in **Figures 7** and **8** and **Table 2**, MC samples demonstrated only moderate improvements in density (increasing from 1.39 to 1.61 g/cm³) and compressive strength (from 2.55 to 11.61 MPa) with increasing sintering temperature. However, these values remained comparatively low, primarily due to persistent porosity (reducing only from 17.01% to 11.36%) and weak ionic diffusion kinetics in the absence of effective fluxing agents. In contrast, MD samples exhibited significantly enhanced densification, with porosity dramatically decreasing to 3.10%, density increasing to 1.92 g/cm³, and compressive strength reaching an impressive 79.01 MPa. This substantial improvement was largely attributed to the formation of transient liquid phases from the inherent Fe_2O_3 and MgO, which effectively facilitated pore elimination and optimal grain rearrangement. Most notably, MH samples consistently achieved the highest performance metrics: An exceptionally low porosity of only 2.90%, a density of 2.30 g/cm³, and a remarkable compressive strength of

110.48 MPa. These values are highly comparable to those reported for mullite synthesized from other industrial wastes (typically ranging from 100 - 300 MPa) [41].

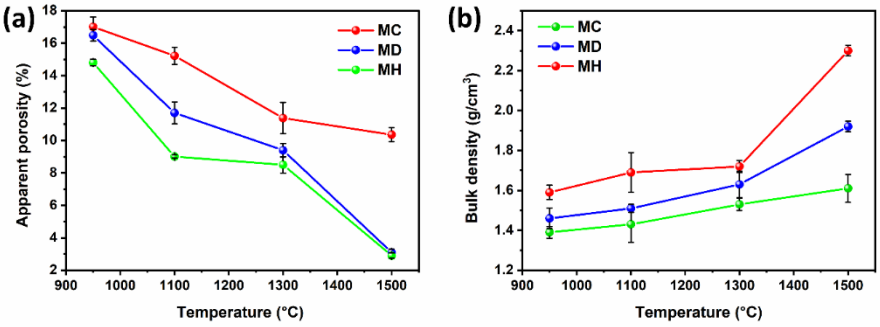

Figure 7 (a) Apparent porosity and (b) bulk density of MC, MD and MH samples at various sintering temperatures.

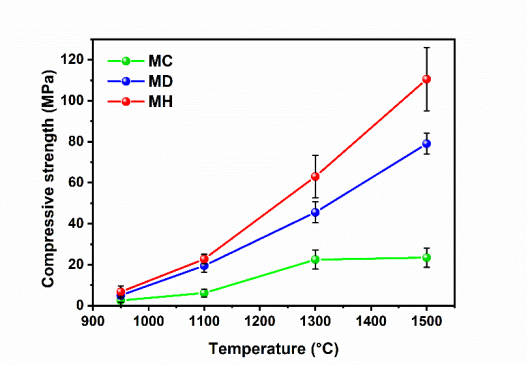

Figure 8 Compressive strength of MC, MD and MH samples as a function of sintering temperature.

Table 2 Apparent porosity, (b) bulk density and compressive stength of MC, MD and MH samples at various sintering temperatures.

Sample	Temperature (℃)	Apparent porosity (%)	Bulk density (g/cm^3)	Compressive strength (MPa)
MC	950 ℃	17.01±0.60	1.39±0.03	2.55±0.90
	1,100 ℃	15.22±0.53	1.43±0.09	6.15±1.95
	1,300 ℃	10.36±0.97	1.53±0.03	22.48±4.67
	1,500 ℃	11.38±0.44	1.61±0.07	23.42±4.71
MD	950 ℃	16.48±0.35	1.46±0.05	5.04±0.32
	1,100 ℃	11.7±0.68	1.51±0.02	19.48±3.19
	1,300 ℃	9.4±0.42	1.63±0.07	45.51±5.11
	1,500 ℃	3.1±0.20	1.92±0.03	79.01±5.07
MH	950 ℃	14.8±0.20	1.59±0.32	6.78±2.81
	1,100 ℃	9.01±0.10	1.69±0.10	22.72±2.32
	1,300 ℃	8.5±0.51	1.72±0.36	62.99±10.28
	1,500 ℃	2.9±0.16	2.3±0.11	110.48±15.44

Collectively, the comprehensive data presented demonstrate that the hydrothermal pretreatment of aluminum dross profoundly enhances its suitability as a primary alumina source for mullite synthesis. By concurrently removing detrimental impurities and converting non-oxide phases into highly reactive

alumina, this method facilitates efficient mullitization under conventional solid-state sintering conditions. The controlled inclusion of specific fluxing oxides within the dross-derived systems further optimizes phase development, ultimately leading to improved mechanical properties that are highly comparable to those of mullite derived from commercial alumina. This innovative approach thus presents a promising avenue for the valorization of industrial waste, effectively transforming a byproduct into a high-value material while concurrently maintaining the critical structural integrity and functional performance required for demanding high-temperature ceramic applications.

Table 3 Mechanical properties as reported by different authors.

Raw materials	Sintering temperature (°C)	Apparent porosity (%)	Bulk density (g/cm^3)	Compressive strength (MPa)	References
Fly ash + alumina sol	1,500	73	0.32	8.0	[42]
Fly ash beads + alumina sol	1,500	-	0.9	4.3	[43]
Fly ash	1,500	56.50±0.07	1.18±0.01	2.10±0.01	[44]
SDA, Kyanite silica fume	1,450	64.78	1.02	22.8	[45]
SAD + red mud	1,450	60.53	1.19	17.77	[37]
Aluminum dross + kaolin	1,500	2.9±0.16	2.3±0.11	110.48±15.44	This work

Conclusions

This study successfully demonstrated a sustainable route for synthesizing high-performance mullite ceramics from aluminum dross and kaolin through hydrothermal pretreatment. Firstly, the hydrothermal pretreatment effectively improved alumina purity and reactivity by removing soluble impurities (e.g., NaCl, AlN) and converting non-oxide aluminum species into reactive Al_2O_3. Secondly, the process enhanced mullite crystallinity, promoted whisker growth, and facilitated densification through the presence of fluxing oxides such as Fe_2O_3 and MgO. Thirdly, the hydrothermally treated composition (MH) achieved superior mechanical properties after sintering at 1,500 °C, with compressive strength of 110 MPa, bulk density of 2.30 g/cm³, and low porosity of 2.90%, outperforming both commercial alumina (MC) and untreated dross (MD).

In summary, this work presents a promising and scalable strategy for the eco-friendly production of mullite. By valorizing aluminum smelting waste through a mild, reagent-free pretreatment process, we offer a viable pathway toward sustainable ceramic manufacturing that reduces reliance on expensive high-purity raw materials and significantly mitigates the growing challenges of industrial waste disposal.

Acknowledgements

We would like to thank the National Research and Innovation Agency through Rumah Program of the Research Organization for Nanotechnology and Materials. This work was partially was supported by the RIIM LPDP Grant and BRIN (grant numbers B-844/II.7.5/FR.06/5/2023 and B-948/III.10/FR.06/5/2023, as well as the Postgraduate Publication Grant FMIPA UI 2025 (grant number PKS-31/UN2.F3.D/PPM.00.02/2024). This research was also supported by the Degree by Research (DBR) scheme of BRIN and access to all characterization equipment was made possible through the National Research and Innovation Agency E-Science Services.

References

[1] H Schneider and S Komarneni. *Mullite*. Wiley-VCH, Weinheim, 2005, p. 1-4.

[2] SG Savio, DA Babu, B Ramakrishna, S Singh and C Vanitha. Influence of sintering process on microstructure and mechanical properties of alumina ceramics: Spark plasma and microwave hybrid sintering. *Ceramics International* 2024; **50(7B)**, 11730-11742.

[3] H Li, H Elsayed and P Colombo. Effect of particle size distribution and printing parameters on alumina ceramics prepared by additive

manufacturing. *Ceramics International* 2024; **50(4)**, 6340-6348.

[4] R Roy, D Das and PK Rout. A review of advanced mullite ceramics. *Engineered Science* 2022; **18**, 20-30.

[5] J Yang, L Tian, L Meng, F Wang, Q Die, H Yu, Y Yang and Q Huang. Thermal utilization techniques and strategies for secondary aluminum dross: A review. *Journal of Environmental Management* 2024; **351**, 119939.

[6] P Ramaswamy, S Ranjit, S Bhattacharjee and SA Gomes. Synthesis of high temperature (1,150 °C) resistant materials after extraction of oxides of Al and Mg from aluminum dross. *Materials Today: Proceedings* 2019; **19(2)**, 670-675.

[7] N Su, Z Li, Y Ding, H Yang, J Zhang and G Fu. Waste to wealth strategy: Preparation and properties of lightweight Al_2O_3-SiO_2-rich castables using aluminum dross waste. *Materials* 2021; **14(24)**, 7803.

[8] PJ Sánchez-Soto, D Eliche-Quesada, S Martínez-Martínez, L Pérez-Villarejo and E Garzón. Study of a waste kaolin as raw material for mullite ceramics and mullite refractories by reaction sintering. *Materials* 2022; **15(2)**, 583.

[9] K Li, S Ge, G Yuan, H Zhang, J Zhang, J He, Q Jia and S Zhang. Effects of V_2O_5 addition on the synthesis of columnar self-reinforced mullite porous ceramics. *Ceramics International* 2021; **47(8)**, 11240-11248.

[10] F Sarraf, E Abbatinali, L Gorjan, T Sebastian, P Colombo, SV Churakov and F Clemens. Effect of MgO sintering additive on mullite structures manufactured by fused deposition modeling (FDM) technology. *Journal of the European Ceramic Society* 2021; **41(13)**, 6677-6686.

[11] YO Raji, MHD Othman, SC Mamah, J Jaafar, MA Rahman, AF Ismail, MH Puteh, TA Kurniawan and KY Wong. TiO_2-embedded dual-layer mullite hollow fiber membranes for efficient removal of persistent organic pollutants from wastewater. *Separation and Purification Technology* 2025; **357(A)**, 130129.

[12] H Majidian, M Farvizi and L Nikzad. Introducing MnO_2 and ZnO additives for the development of alumina–mullite–zirconia composites. *Journal of The Minerals, Metals & Materials Society* 2021; **73(11)**, 3486-3496.

[13] S Kamara, Y Ma, EH Foday and HDS Kallon. Synthesis of mullite ceramics from powdered mine tailings reinforced with Al_2O_3. *International Journal of Applied Ceramic Technology* 2025; **22(2)**, e14932.

[14] Y Liu, W Lian, W Su, J Luo and L Wang. Synthesis and mechanical properties of mullite ceramics with coal gangue and wastes refractory as raw materials. *International Journal of Applied Ceramic Technology* 2020; **17(1)**, 205-210.

[15] K Tabit, W Borja, L Saâdi and M Waqif. Low-temperature synthesis of mullite-based ceramics from Moroccan naturally occurring andalusite and marble waste. *International Journal of Applied Ceramic Technology* 2022; **19(3)**, 1274-1280.

[16] M Mahinroosta and A Allahverdi. Hazardous aluminum dross characterization and recycling strategies: A critical review. *Journal of Environmental Management* 2018; **223**, 452-468.

[17] A Meshram and KK Singh. Recovery of valuable products from hazardous aluminum dross: A review. *Resources, Conservation and Recycling* 2018; **130**, 95-108.

[18] A Gil and SA Korili. Management and valorization of aluminum saline slags: Current status and future trends. *Chemical Engineering Journal* 2016; **289**, 74-84.

[19] HL Yang, ZS Li, YD Ding, QQ Ge, YJ Shi and L Jiang. Effect of silicon source (fly ash, silica dust, gangue) on the preparation of porous mullite ceramics from aluminum dross. *Materials* 2022; **15(20)**, 7212.

[20] C Li, W Liu, F Jiao, L Dong, S Liu and W Qin. Intensifying recovery of metallic aluminum in secondary aluminum dross by alkali roasting-water leaching. *Transactions of Nonferrous Metals Society of China* 2024; **34(12)**, 4063-4074.

[21] CT Foo, MAM Salleh, KK Ying and KA Matori. Mineralogy and thermal expansion study of mullite-based ceramics synthesized from coal fly ash and aluminum dross industrial wastes. *Ceramics International* 2019; **45(6)**, 7488-7494.

[22] MF Zawrah, AR Wassel, RA Youness and MA Taha. Recycling of aluminum dross and silica fume wastes for production of mullite-containing

ceramics: Powder preparation, sinterability and properties. *Ceramics International* 2022; **48(21)**, 31661-31671.

[23] X Xu, Y Shen, Z Zhang, J Wu, J Yu and Y Zhou. Influence of Fe_2O_3 on the absorptivity of in situ synthesized solar high-temperature absorbing and storing integrated mullite-based ceramics. *Ceramics International* 2024; **50(15)**, 27339-27348.

[24] P Kumar, M Nath, A Ghosh and HS Tripathi. Thermo-mechanical properties of mullite-zirconia composites derived from reaction sintering of zircon and sillimanite beach sand: Effect of CaO. *Transactions of Nonferrous Metals Society of China* 2016; **26(9)**, 2397-2403.

[25] N Sadli, A May, M Hamidouche, A Henniche, H Belhouchet and H Boudouh. Investigations on kaolin mixtures: Impact on mullite formation kinetics and microstructure evolution. *International Journal of Applied Ceramic Technology* 2024; **21(6)**, 3950-3966.

[26] H Feng, Y Liu and Q Jin. Effect of in-situ nano-alumina on the properties of alumina ceramics from secondary aluminum dross. *Ceramics International* 2024; **50(22B)**, 46227-46238.

[27] M Shi, Y Li and J Shi. Fabrication of periclase and magnesium aluminate spinel refractory from washed residue of secondary aluminum dross. *Ceramics International* 2022; **48(6)**, 7668-7676.

[28] R Salomão, L Fernandes and NCM Spera. Combined effects of SiO_2 ratio and purity on physical properties and microstructure of in situ alumina-mullite ceramic. *International Journal of Applied Ceramic Technology* 2021; **18(5)**, 1702-1709.

[29] X Huang, X Yang and X Wang. Thermodynamic properties of aluminum titanate-mullite composite ceramics containing heat stabilizer. *International Journal of Applied Ceramic Technology* 2023; **20(5)**, 2974-2984.

[30] Z Li, H Li, X Huang, W Wu, Z Sun, X Wu and S Li. Removal of nitrides and fluorides from secondary aluminum dross by catalytic hydrolysis and its mechanism. *Heliyon* 2023; **9(1)**, e12893.

[31] A Olanrewaju, AK Oluseyi and SK Das. The effect of MgO and Cr2O3 on mullite formation from Nigeria sourced kaolin-calcined alumina sintered compacts. *IOP Conference Series: Materials Science and Engineering* 2019; **509**, 012007.

[32] A Srivastava and A Meshram. On trending technologies of aluminium dross recycling: A review. *Process Safety and Environmental Protection* 2023; **171**, 38-54.

[33] Y Mochizuki and N Tsubouchi. Co-processing method for the stabilization of aluminum dross and the production of valuable substrates via hydrothermal treatment. *ACS Sustainable Chemistry & Engineering* 2024; **12(13)**, 5263-5271.

[34] A Esharghawi, C Penot and F Nardou. Contribution to porous mullite synthesis from clays by adding Al and Mg powders. *Journal of the European Ceramic Society* 2009; **29(1)**, 31-38.

[35] DH Piva, RH Piva, J Venturini, J Ramon, V Caldas, MR Morelli and CP Bergmann. Effect of Fe_2O_3 content on the electrical resistivity of aluminous porcelain applied to electrical insulators. *Ceramics International* 2016; **42(4)**, 5045-5052.

[36] SGD Iya, MZ Noh, SNA Razak, N Sharip and NAA Kutty. Effect of iron (111) oxide (Fe_2O_3) as an additive and substitution of quartz with POFA on physico-mechanical properties of porcelain. *International Journal of Nanoelectronics and Materials* 2019; **12(2)**, 175-184.

[37] B Lou, H Shen, B Liu, J Zhang, X Zhang, J Liu and S Zhang. In-situ preparation of porous metal-ceramic composite from secondary aluminum dross and red mud for adsorption of organic pollutant. *Journal of Alloys and Compounds* 2024; **986**, 174135.

[38] S Ilić, S Zec, M Miljković, D Poleti, M Pošarac–Marković, D Janćković and B Matrović. Sol-gel synthesis and characterization of iron doped mullite. *Journal of Alloys and Compounds* 2014; **612**, 259-264.

[39] VJ Silva, MF Silva, WP Gonçalves, RRD Menezes, GDA Neves, HDL Lira and LNDL Santana. Porous mullite blocks with compositions containing kaolin and alumina waste. *Ceramics International* 2016; **42(14)**, 15471-15478.

[40] RH Piva, P Vilarinho, MR Morelli, MA Fiori and ORK Montedo. Influence of Fe_2O_3 content on the

dielectric behavior of aluminous porcelain insulators. *Ceramics International* 2013; **39(7)**, 7323-7330.

[41] TF Choo, MAM Salleh, KY Kok and KA Matori. A review on synthesis of mullite ceramics from industrial wastes. *Recycling* 2019; **4(3)**, 39.

[42] M Li, P Li, Q Gao, S Li, R Chen, H Wen and C Li. Fly ash coated with alumina sol for improving strength and thermal insulation of mullite porous ceramics. *Construction and Building Materials* 2024; **416**, 135013.

[43] S Li, J Xin and R Chen. Achieving high strength and low thermal conductivity: Additive manufacturing of mullite lightweight refractory. *Ceramics International* 2024; **50(16)**, 27880-27888.

[44] B Xia, Z Wang, L Gou, M Zhang and M Guo. Porous mullite ceramics with enhanced compressive strength from fly ash-based ceramic microspheres: Facile synthesis, structure, and performance. *Ceramics International* 2022; **48(8)**, 10472-10479.

[45] L Dong, H Chen, X Zeng, X Chen, W Fang, X Du, Z Huang, X He, W Li, D Wang and L Zhao. Porous ceramics with low thermal conductivity from hazardous secondary aluminum dross. *Construction and Building Materials* 2025; **489**, 142162.